UNIVERSIDAD NACIONAL DE COLOMBIA
SEDE MEDELLÍN
FACULTAD DE MINAS

DYNA
http://dyna.medellin.unal.edu.co/

Modeling attenuation and dispersion of acoustic waves in porous media containing immiscible non viscous fluids

Alejandro Duitama-Leal [a], Ovidio Almanza [b] & Luis Montes-Vides [c]

[a] *Departamento de Matemáticas, Universidad de Cundinamarca, Bogotá, Colombia, adulfisica@gmail.com.*
[b] *Departamento de Física, Universidad Nacional de Colombia, Bogotá, Colombia. oaalmanzam@unal.edu.co*
[c] *Departmento de Geociencias, Universidad Nacional de Colombia, Bogotá, Colombia. lamontesv@unal.edu.co*

Received. March 16th, 2016. Received in revised form. August 12th, 2016. Accepted. September 2nd, 2016.

Abstract
This paper reports the results of the propagation of P-waves in porous media, simulated by solving the generalized Biot´s equations in finite differences. In saturated models, it was observed that when a wave advances, the maximum amplitude of the spectrum is shifted to lower frequencies, and that this maximum amplitude and its frequency are directly related. Besides this, the quality factor decreases with porosity and saturation. Hence, attenuation becomes higher when porosity, saturation, and frequency increase but tends asymptotically towards a constant value. Although phase analysis is generally discarded, it does provide interesting results. It was noted that the wave phase changes linearly with frequency at a rate of change that increases linearly with travel time. This rate increases with saturation but decreases slightly with porosity. This work ignores spherical divergence or scattering and concentrates on intrinsic attenuation caused by friction, particularly between fluids and solid particles.

Keywords. Biot theory, attenuation, viscosity, saturation, porosity.

Modelado de atenuación y dispersión de ondas acústicas en medios porosos que contienen fluidos inmiscibles no viscosos

Resumen
Este artículo reporta resultados de la propagación de ondas P en medios porosos, simulada solucionando en diferencias finitas las ecuaciones generalizadas de Biot. En modelos saturados se observó que cuando avanza la onda, la amplitud máxima del espectro se desplaza hacia frecuencias menores, y que esta amplitud máxima y su frecuencia están directamente relacionadas. Además, que el factor de calidad disminuye con la porosidad y la saturación. Por ende, la atenuación aumenta con la porosidad, la saturación y la frecuencia pero tiende asintóticamente a un valor constante. Se observó que la fase de la onda cambia linealmente con la frecuencia a una rata de cambio que aumenta linealmente con el tiempo de viaje. Esta rata aumenta con la saturación pero disminuye ligeramente con la porosidad. Este trabajo ignora la divergencia esférica y la retro dispersión, concentrándose en la atenuación intrínseca causada por la fricción, en particular entre líquido y partículas sólidas.

Palabras clave. Teoría de Biot; atenuación; viscosidad; saturación; porosidad.

1. Introduction

Attenuation is the exponential decay of traveling wave amplitude and dispersion is the change of velocity with frequency. These can be used to enhance seismic resolution and as direct hydrocarbon indicators. The intrinsic attenuation is quantified by the inverse of the quality factor Q^{-1} as the fraction of wave energy transformed to heat in each period, whereas the attenuation scattering Q_{scat}^{-1} is due to energy scattered in all directions. The sum of both is known as total attenuation. In mild stratified sediments, the scattering losses are considered negligible depending on

How to cite: Duitama-Leal, A., Almanza, O. & Montes-Vides, L. Modeling attenuation and dispersion of acoustic waves in porous media containing immiscible non viscous fluids DYNA 83 (199) pp. 78-85, 2016

frequency range, varying the relation Q^{-1}/Q_{scat}^{-1} from 19 in sonic logs to 4 in VSP (Vertical Seismic Profile) [1]. In sedimentary environments, Q^{-1} values ranging from 10^{-2} to 10^{-1} across the seismic band (1-150 Hz) have been reported [1].

Despite scientific improvements, the physical phenomena related to the intrinsic and scattering attenuations in sedimentary rocks are not completely understood. Notwithstanding different flow regimes and frequency bands, it is possible to explain some aspects of wave attenuation with a single mechanism. wave induced fluid flow - WIFF. When a wave stresses an average element, pore fluids respond with different changes in their fluid pressures. As a consequence, fluids within the porous element start flowing, significantly attenuating the wave energy. It has been demonstrated that these fluid-flow waves are responsible for dispersion and attenuation at low frequencies (31-123 Hz) [2]. Additionally, the relative motion between the rock matrix and the fluids is intensified by the presence of fluid-fluid interfaces and their pressure gradients [3]. It has been demonstrated that WIFF causes significant attenuation in partially saturated Berea sandstone at low and high pressure [4]. The induced flows take place at distinct scales, the macroscopic scale phenomenon at low or high frequencies is known as “Biot loss” [5,6]. Microscopic mechanisms caused by micro-cracks or broken grain contact under stress and known as squirt flow have been proposed to explain measured attenuation at ultrasonic frequencies [7-9]. Also, mesoscopic mechanisms have been reported [10] to treat wave induced flow due to patchy saturation. Pride and Berryman [11,12] published research on mesoscopic losses occurring in the double-porosity model. At low rates of varying strain and at a larger length scale compared to typical pore size, the fluid pressure has enough time to equilibrate between the porous phases and consequently, the double porosity model is reduced to the Biot one porosity mechanism [13]. It is even believed that at seismic frequencies the main cause is the WIF; in homogeneous media, WIF becomes weaker and Biot loss could be sizeable. On the other hand, understanding the effects of saturation and viscosity on seismic response requires numerical simulations given that laboratory tests must be carried out with strains and frequencies set in the seismic domain. Hence, the propagation of acoustic waves in wet porous media was numerically simulated. Biot´s equations were extended to porous media saturated with two immiscible fluids [14], solved in finite differences and coded in a C++ program. These equations include a complex quantity that represents the deviation from Poiseuille friction as the frequency increases, transforming the static viscosity coefficient into a dynamic complex term. Models with variable porosity and saturation were used to discriminate their separated effects of porosity and saturation. Spectral analysis using Fourier transform provided information about the behavior of amplitude and phase spectra of wavelets (although phase analysis is mostly disregarded) that characterize seismic response within these two parameters.

2. Theory

2.1. Wave propagation in porous media

The stresses and strains of the material inside a continuous elastic volume are connected by the Hooke's law, which only holds for some materials under certain loading conditions. Under these circumstances, the second-order tensors that represent stress and strain are related through a fourth-rank stiffness tensor.

Now, consider a homogeneous and isotropic volume of rock δv with porosity β and density ρ_{11}, which contains two immiscible fluids with saturation *S* and (*S-1)* and respective densities ρ_{22} and ρ_{33}. The displacements of the solid, and fluids 1 and 2 are designated by the independent vectors $\vec{u} = (u_x, u_y, u_z)$, $\overrightarrow{U} = (U_x, U_y, U_z)$ and $\vec{V} = (V_x, V_y, V_z)$.

When a wave propagates across a media, the faces of the solid volume are under the stress tensor

$$\sigma_{ij} = \begin{bmatrix} \sigma_{xx} & \sigma_{xy} & \sigma_{xz} \\ \sigma_{yx} & \sigma_{yy} & \sigma_{yz} \\ \sigma_{zx} & \sigma_{zy} & \sigma_{zz} \end{bmatrix} \quad (1)$$

and the surfaces of fluids 1 and 2 are under forces which are proportional to the fluids pressure $-p$ according to.

$$F_1 = -p\beta S \quad (2)$$

$$F_2 = -p\beta(1 - S) \quad (3)$$

The minus sign indicates that the force is exerted in the opposite direction to the pressure.

The following strain tensor represents the deformed porous solid

$$e_{ij} = \begin{bmatrix} e_{xx} & e_{xy} & e_{xz} \\ e_{yx} & e_{yy} & e_{yz} \\ e_{zx} & e_{zy} & e_{zz} \end{bmatrix} \quad (4)$$

with $e_{xx} = \partial u_x/\partial x$, $e_{xy} = \partial u_x/\partial y$, $e_{xz} = \partial u_x/\partial z$, $e_{yx} = \partial u_y/\partial x$, $e_{yy} = \partial u_y/\partial y$, $e_{yz} = \partial u_y/\partial z$, $e_{zx} = \partial u_z/\partial x$, $e_{zy} = \partial u_z/\partial y$ and $e_{zz} = \partial u_z/\partial z$.

The changes of volume in fluids 1 and 2 are

$$e_1 = \frac{\partial U_x}{\partial x} + \frac{\partial U_y}{\partial y} + \frac{\partial U_z}{\partial z} \quad (5)$$

$$e_2 = \frac{\partial V_x}{\partial x} + \frac{\partial V_y}{\partial y} + \frac{\partial V_z}{\partial z} \quad (6)$$

The kinetic energy of the system E_k per unit of volume is estimated by.

$$2E_{Kinetic} = \begin{bmatrix} \rho_{11}\left(\left(\frac{\partial u_x}{\partial t}\right)^2+\left(\frac{\partial u_y}{\partial t}\right)^2+\left(\frac{\partial u_z}{\partial t}\right)^2\right)+ \\ \rho_{22}\left(\left(\frac{\partial U_x}{\partial t}\right)^2+\left(\frac{\partial U_y}{\partial t}\right)^2+\left(\frac{\partial U_z}{\partial t}\right)^2\right)+ \\ \rho_{33}\left(\left(\frac{\partial V_x}{\partial t}\right)^2+\left(\frac{\partial V_y}{\partial t}\right)^2+\left(\frac{\partial V_z}{\partial t}\right)^2\right)+ \\ 2\rho_{12}\left(\frac{\partial u_x}{\partial t}\frac{\partial U_x}{\partial t}+\frac{\partial u_y}{\partial t}\frac{\partial U_y}{\partial t}+\frac{\partial u_z}{\partial t}\frac{\partial U_z}{\partial t}\right)+ \\ 2\rho_{13}\left(\frac{\partial u_x}{\partial t}\frac{\partial V_x}{\partial t}+\frac{\partial u_y}{\partial t}\frac{\partial V_y}{\partial t}+\frac{\partial u_z}{\partial t}\frac{\partial V_z}{\partial t}\right) \end{bmatrix} \quad (7)$$

$\rho_{11}\left(\left(\frac{\partial u_x}{\partial t}\right)^2+\left(\frac{\partial u_y}{\partial t}\right)^2+\left(\frac{\partial u_z}{\partial t}\right)^2\right)$,$\rho_{22}\left(\left(\frac{\partial U_x}{\partial t}\right)^2+\left(\frac{\partial U_y}{\partial t}\right)^2+\left(\frac{\partial U_z}{\partial t}\right)^2\right)$ and $\rho_{33}\left(\left(\frac{\partial V_x}{\partial t}\right)^2+\left(\frac{\partial V_y}{\partial t}\right)^2+\left(\frac{\partial V_z}{\partial t}\right)^2\right)$

corresponds to the kinetic energy of the matrix, and the kinetic energy of fluids 1 and 2, respectively. The mass coefficients ρ_{12} and ρ_{13} are apparent densities which represent coupling parameters between the fluids and the solid, so the last two terms correspond to their coupling energies. The weak gas-liquid interaction was not taken into account. As a result, the friction is only due to the relative motion between the solid and every fluid, and the dissipation function D becomes.

$$D = \frac{b}{2}\begin{bmatrix} \left(\frac{\partial u_x}{\partial t}-\frac{\partial U_x}{\partial t}\right)^2+\left(\frac{\partial u_y}{\partial t}-\frac{\partial U_y}{\partial t}\right)^2+\left(\frac{\partial u_z}{\partial t}-\frac{\partial U_z}{\partial t}\right)^2+ \\ \left(\frac{\partial u_x}{\partial t}-\frac{\partial V_x}{\partial t}\right)^2+\left(\frac{\partial u_y}{\partial t}-\frac{\partial V_y}{\partial t}\right)^2+\left(\frac{\partial u_z}{\partial t}-\frac{\partial V_z}{\partial t}\right)^2 \end{bmatrix} \quad (8)$$

where b is the Darcy´s coefficient of the fluid component that relates the total friction force on the fluid with the average fluid velocity and depends on the fluid´s dynamic viscosity γ, the permeability κ, and the porosity β of the matrix, according to.

$$b = \frac{\gamma\beta^2}{\kappa}, \quad (9)$$

b depends on the fluids hence $b = b_1 + b_2$, where $b_1 = \gamma_1(\beta S)^2/\kappa$ and $b_2 = \gamma_2(\beta(1-S))^2/\kappa$ are the individual Darcy coefficients of each fluid. After a certain frequency f_L given later by equation (19), fluids behave as a non-laminar or Poiseuille flow, hence D in equation (8) must be multiplied by the factor

$$F(\Gamma) = \frac{F}{(\delta\sqrt{(f(\rho_{12}+\rho_{22}+\rho_{13}+\rho_{33})/(4\sqrt{2}b)})} \quad (10)$$

$\Gamma = \sqrt{f/f_L}$ represents the ratio between angular frequency and critical frequency f_L, δ is a structure factor which depends on pore geometry, and ρ_{12}, ρ_{22}, ρ_{13} and ρ_{33} are defined by.

$$\rho_{22} = c\rho_1\beta S,\ \rho_{12} = \rho_1\beta S(1-c),\ \rho_{13} = \rho_2\beta(1-S)(1-c),\ \rho_{33} = c\rho_2\beta(1-S)$$

The propagation of waves across the porous matrix saturated by the immiscible fluids is governed by the system of coupled equations.

$$\begin{bmatrix} \mu\vec{\nabla}^2\vec{u}+ \\ (\lambda+2\mu)\vec{\nabla}(\vec{\nabla}\cdot\vec{u})+ \\ +Q_1\vec{\nabla}(\vec{\nabla}\cdot\vec{U})+ \\ +\vec{\nabla}(\vec{\nabla}\cdot\vec{V}) \end{bmatrix} = \begin{bmatrix} \frac{\partial^2}{\partial t^2}(\rho_{11}\vec{u}+\rho_{12}\vec{U}+\rho_{13}\vec{V})+ \\ bF(\Gamma)\frac{\partial}{\partial t}(\vec{u}-\vec{U})+ \\ bF(\Gamma)\frac{\partial}{\partial t}(\vec{u}-\vec{V}) \end{bmatrix} \quad (11)$$

$$\begin{bmatrix} Q_1\vec{\nabla}(\vec{\nabla}\cdot\vec{u})+ \\ R_1\vec{\nabla}(\vec{\nabla}\cdot\vec{U}) \end{bmatrix} = \begin{bmatrix} \frac{\partial^2}{\partial t^2}(\rho_{22}\vec{U}+\rho_{12}\vec{u})- \\ bF(\Gamma)\frac{\partial}{\partial t}(\vec{u}-\vec{U}) \end{bmatrix} \quad (12)$$

$$\begin{bmatrix} Q_1\vec{\nabla}(\vec{\nabla}\cdot\vec{u})+ \\ R_1\vec{\nabla}(\vec{\nabla}\cdot\vec{V}) \end{bmatrix} = \begin{bmatrix} \frac{\partial^2}{\partial t^2}(\rho_{33}\vec{V}+\rho_{13}\vec{u})- \\ bF(\Gamma)\frac{\partial}{\partial t}(\vec{u}-\vec{U}) \end{bmatrix} \quad (13)$$

The displacements vectors $\vec{u} = (u_x, u_y, u_z)$, $\overrightarrow{U} = (U_x, U_y, U_z)$ and $\vec{V} = (V_x, V_y, V_z)$ are completely described by the nine independent equations 11, 12 and 13. In isotropic material, the transverse and longitudinal waves are uncoupled and they obey independent equations of propagation. The terms D_1, R_1, R_2, $Q_1$and Q_2 in equations 11, 12 and 13 are defined below.

$$D_1 = K_s\left[1+\beta S\left(\frac{K_S}{K_1}-1\right)+\beta(1-S)\left(\frac{K_S}{K_2}-1\right)\right] \quad (14)$$

$$R_1 = s\left(\frac{\beta K_S}{D_1-K_b}\right)^2 \quad (15)$$

$$R_2 = (1-s)\left(\frac{\beta K_S}{D_1-K_b}\right)^2 \quad (16)$$

$$Q_1 = \beta S\left(\frac{K_S(K_S-K_b)}{D_1-K_b}-\frac{{K_S}^2}{D_1-K_b}\beta\right) \quad (17)$$

$$Q_2 = \beta(1 - S(\frac{K_S(K_S - K_b)}{D_1 - K_b} - \frac{{K_S}^2}{D_1 - K_b}\beta) \quad (18)$$

μ is the shear modulus, K_b is the Bulk Modulus of the Structure and λ is the second Lame´s parameter, R_1 and R_2 represent the pressure on fluids 1 or 2 required to displace the fluids into the porous, and Q_1 and Q_2 are physical constants that provide information about the solid-fluids couplings. K_1 and K_2 are the bulk modulus of the fluid 1 and 2, and K_s is the bulk modulus of the sand (grains).

In a porous material with an average pore diameter of d, the Poiseuille flow occurs below a certain frequency f_L that defines the low frequency bandwidth [5]. Such a frequency is given by.

$$f_L = (\pi\gamma)/(4d^2) \quad (19)$$

The longitudinal waves are decoupled from transverse waves, by applying the divergence operator on both sides of equations (11), (12) and (13) to finally obtain.

$$\begin{bmatrix} (\lambda + 2\mu)\vec{\nabla}^2 e + \\ Q_1\vec{\nabla}^2 e_1 + \\ Q_2\vec{\nabla}^2 e_2 \end{bmatrix} = \begin{bmatrix} \frac{\partial^2}{\partial t^2}(\rho_{11}e + \rho_{12}e_1 + \rho_{13}e_2) + \\ bF(\Gamma)\frac{\partial}{\partial t}(e - e_1) + \\ bF(\Gamma)\frac{\partial}{\partial t}(e - e_2) \end{bmatrix} \quad (20)$$

$$\begin{bmatrix} Q_1\vec{\nabla}^2 e + \\ R_1\vec{\nabla}^2 e_1 \end{bmatrix} = \begin{bmatrix} \frac{\partial^2}{\partial t^2}(\rho_{22}e_1 + \rho_{12}e) - \\ bF(\Gamma)\frac{\partial}{\partial t}(e - e_1) \end{bmatrix} \quad (21)$$

$$\begin{bmatrix} Q_2\vec{\nabla}^2 e + \\ R_2\vec{\nabla}^2 e_2 \end{bmatrix} = \begin{bmatrix} \frac{\partial^2}{\partial t^2}(\rho_{33}e_2 + \rho_{13}e) - \\ bF(\Gamma)\frac{\partial}{\partial t}(e - e_2) \end{bmatrix} \quad (22)$$

The set of equations 20, 21 and 22 rule the propagation of longitudinal waves in porous media containing fluids. The extension of this theory to the high-frequency range was developed by Biot [6], and since then it has been widely used in petroleum engineering.

A more detailed explanation of Biot´s theory can be found in reference [14,15].

2.2. Attenuation and Dispersion

Intrinsic seismic attenuation is characterized by the quality factor Q, defined in terms of the mean stored energy W divided by the energy lost δW during a cycle of sinusoidal deformation. The lost energy is absorbed by the medium as heat energy. Q quantifies the attenuation caused by fluid movement and friction in pores, and is related to the phase angle ϑ between stress and strain, according to

$$Q^{-1} = tan(\vartheta) \quad (23)$$

As is known, the Earth's crust preferentially attenuates higher frequencies, diminishing the seismic resolution.

Wavelets are formed by superposing monochromatic waves called frequency components of the wave, where each component travels with a velocity called phase velocity that depends on its frequency. Dispersion is the phenomenon by which each component has a different phase velocity that distorts the shape of the wave. When this occurs, the medium is referred to as dispersive.

3. Methodology

The system of simultaneous differential equations (20), (21) and (22), solved in the second order central finite difference scheme, was implemented in a C++ code. Porous sandstones were modeled as homogeneous isotropic porous media containing non-viscous fluids (gas and water). Each model with a different porosity and a distinct saturation according to its mechanical properties is listed in Table 1. To eliminate ghost reflections in the lateral and inferior regions bordering the model, non-reflecting borders were included by implementing Perfectly Matched Layers (PML) [16]. The efficiency of PML borders surrounding the model is observed in Fig. 1A containing three snapshots. the first at t=5 ms, the second at t=15 ms with spurious reflections on the borders, and the third at t=15 ms without reflections on PML borders. In order to circumvent geometric dispersion, the source generates a plane wave on the model simulating a 60Hz Ricker wavelet. In each simulation, the wave propagated in a 2D model with a depth of 2km and a width of 0.05 km formed grids that were 0.5 m high and 0.5 m thick. The downward wave was recorded at 20 points with a separation of 100 meters between one recording position and the next. The simulation time was 350 milliseconds and the sampling rate, 50 microseconds. According to equation (14), and taking into account the values listed in Table 1, the estimated critical frequency values are in kHz, hence the bandwidth of simulations is located in the seismic frequency range. To observe the isolated effect of porosity on attenuation and dispersion, some numerical simulations ran in fully saturated models each one with a different porosity. With that intention, homogeneous models saturated with water at 99.9% were created, with porosities varying of between 2.5% and 22.5% and with increases of 2.5%. Similarly, to observe the isolated effect of saturation on attenuation, other numerical simulations were run in constant porosity models with different saturations, ranging from 10% to 99.9%, with increases of 10%. For each simulation, the wavelets recorded in depth in each model, were spectrally decomposed by Fourier transform providing their respective amplitude and phase spectra. Besides the above, arrival times were estimated to find out the combined effect of porosity and saturation in P-wave velocity.

Table 1
Mechanical properties of model with pore containing gas and water.

Properties	Sandstone	Water	Gas
Density [kg/m^3]	2650	1000	1.21
Grain Bulk modulus [GPa]	20	2	1.42 x 10^{-4}
Dynamic viscosity [Pa-s]		1 x 10^3	1.81 x 10^{-5}
Porosity [%]	$0< \beta < 40$		
Saturation [%]		10 <S< 99.9	
Shear modulus [MPa]	26.1		
Dynamic permeability [m^2]	$10^{-8} < \chi < 10^{-12}$		
Grain size [m]	5 x 10^{-4}		
Pore tortuosity	1.25		
Shear modulus structure [N/ m^2]	2.61X10^7		
Bulk modulus structure [N/ m^2]	4.36X10^7		

Source. The authors.

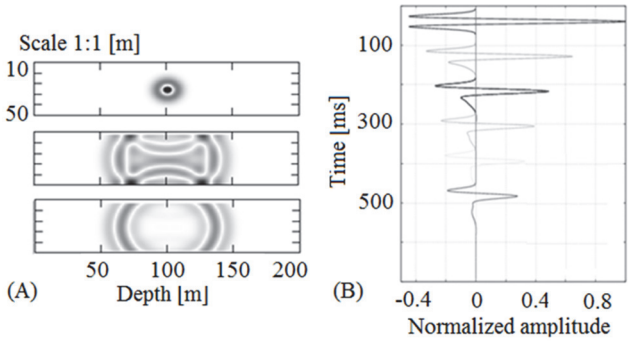

Figure 1. A) At top, In the first snapshot, 5 ms after source activation, in the second snapshot, 10 ms later with strong reflections on upper and lower borders and in the third snapshot, absence of ghost reflections due to the non-reflecting PML borders. B) Wavelets recorded at different depths with decreasing amplitudes and changing waveform.
Source. The authors.

3.1. Analysis of results

Fig. 1B depicts a synthetic seismogram formed by six superimposing wavelets recorded in depth in a 15% porosity model of a porous sandstone which is saturated with water at 99.9%, where the attenuation is manifested by a reduction of the amplitudes, while the dispersion is manifested by changing the waveforms. In a perfectly elastic homogeneous-isotropic medium, all frequency components travel with the same phase velocity without energy loss and, as a result, the wavelet holds its form while moving. The six wavelets of Fig. 1A were Fourier transformed and their amplitude spectra plotted in Fig. 2A, indicating the depth at which each wavelet was recorded. The image shows the amplitude spectrum diminishing in depth whereas the higher amplitude A_m of each spectrum is shifted toward low frequencies; from now on, the frequency of the maximum component energy of each spectrum will be referred to as f_m. On the surface, f_m is 60 Hz but at 100 m depth, it is 47 Hz. It reaches 45 Hz at 200 m; simultaneously the shape of the spectrum is continuously modified until it becomes bi-modal at 600m. Given that the plane wave does not suffer geometric dispersion, the above observed behavior is associated entirely to the friction by the relative motion between the fluids and the pore wall. Fig. 2B contains the phase spectra of wavelets recorded at depths of 100, 200 and 400 m. The phase spectra indicate that phase and frequency are related by the expression $\emptyset(\boldsymbol{\omega}) = \emptyset_0 + \boldsymbol{m(z)\omega}$, where the ratio of change of phase with frequency $\boldsymbol{m(z)} = \frac{\partial \emptyset}{\partial \boldsymbol{\omega}}$ increases in depth z. The above procedure, including wave propagation, wavelet recording in depth, and spectral analysis, was repeated for all numerical simulations.

Now, to quantify the impact of porosity on attenuation and dispersion, the wavelets recorded in depth and supplied by the simulation in each model were spectrally decomposed using the Fourier transform. As stated, each saturated model has a different porosity. From now on, the spectra of wavelets recorded in depth will be referred to as spectra in depth. Accordingly, the spectra in depth of each model were overlapped as shown in Fig. 2. Next, the logarithms of measured amplitudes at 40, 50, 60, 70, and 80 Hz were normalized by dividing each value by the maximum value, as shown in Fig. 3A. Each curve indicates that attenuation becomes stronger with porosity, which is explained by the fact that the pore surface, where friction occurs, is extended when porosity increases. Also, by comparing the curves according to frequency, it can be deduced that attenuation caused by porosity is strengthened when frequency increases.

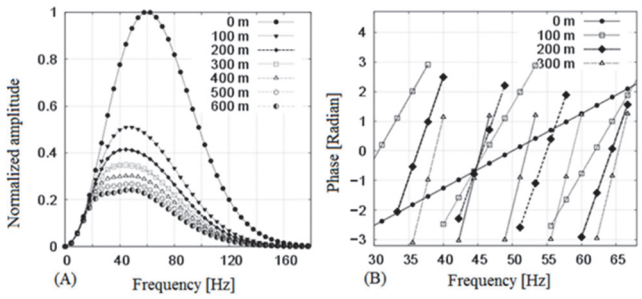

Figure 2 A) Amplitude spectra of source and wavelets recorded at depths of 100, 200, 300, 400, 500 and 600 m where the attenuation of high frequency components is evident. B) Phase spectra of wavelets at depths of 0, 100, 200 and 300 m, with each one showing a linear relationship between the phase and frequency.
Source. The authors.

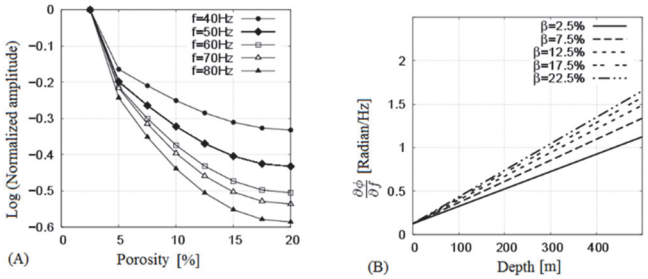

Figure 3 A) Variation of amplitudes for different frequency components as a function of porosity. B) Variation of phase with frequency ($\partial\emptyset$)/(∂f)) increases linearly with time with the rate exacerbated by porosity.
Source. The authors.

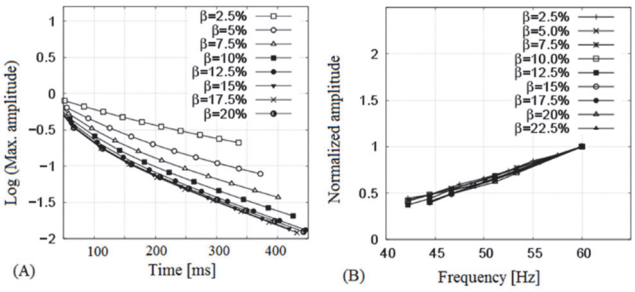

Figure 4. A) Decay of the amplitude with porosity measured at different depths. B) A linear relationship between normalized A_m and f_m which depends weakly on porosity.
Source. The authors

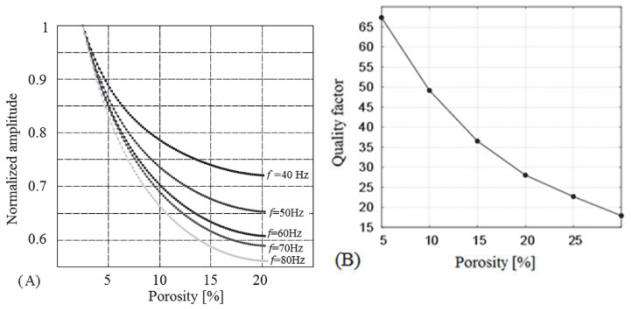

Figure 5 A) Normalized amplitude decays exponentially with porosity, and increases with frequency. B) Quality factor Q of 60Hz frequency component estimated in different constant porosity models, with a nonlinear relation that decreases according to increases in porosity β.
Source. The authors.

This can be explained by the following fact. At low frequencies, there is a partial coupling between fluids and the solid but at higher frequencies, the coupling breaks and friction increases together with the energy transfer rate. In order to find the effects of porosity on dispersion, $\boldsymbol{m(z) = \partial\emptyset/\partial f}$ were measured in phase spectra in depth of each model with a different porosity. The summarized results are shown in Fig. 3B. Fig. 2B shows that in a homogeneous-isotropic saturated media, $\boldsymbol{m(z)}$ increases with depth, whereas Fig. 3B shows that $\boldsymbol{m(z)}$ becomes higher when porosity increases, exacerbating the dispersion phenomena. The term $\boldsymbol{m(z) = \partial\emptyset/\partial f}$ might be considered a seismic attribute and therefore a porosity indicator inside a fully saturated lithic unit, relating their values directly with their porosities.

On the other hand, the highest amplitudes of all spectra in depth were estimated. Fig. 4A shows curves relating the logarithm of the highest amplitudes $\boldsymbol{A_m}$ versus travel time and porosity. Each curve shows an exponential decay of amplitude with the travel time and a decay factor which increases with porosity. Although attenuation increases with porosity, the lines tend asymptotically to a limiting line established in this modeling by a porosity of about 22.5%. This means that above this value, attenuation will remain constant no matter what the value of porosity is.

Fig. 1B illustrates that the maximum amplitude $\boldsymbol{A_m}$ shifts to lower frequencies when the depth increases. Therefore, the highest amplitudes ($\boldsymbol{A_m}$) of all spectra in depth and their frequencies ($\boldsymbol{f_m}$) were estimated and plotted in Fig. 4B. A numerical regression indicates a linear relation between $\boldsymbol{A_m}$ and $\boldsymbol{f_m}$ which is almost insensitive to porosity. In a real case, the dispersion around the relationship would be below estimation errors. The next step was to consider the quality factor Q, so the amplitudes at 40, 50, 60, 70 and 80 Hz of all spectra in depth versus porosity were plotted. Fig. 5A shows how amplitude decreases exponentially with porosity and increases with frequency. It means that the higher frequency components of waves are rapidly attenuated while the low frequency components remain. The amplitudes of the 60Hz component were plotted in Fig. 5B, which shows the decreasing effect of porosity on quality factor. Q tends asymptotically to a constant value, as porosity increases. Values from Fig. 5A were used to build the curves associated to components of 40, 50, 70 and 80 Hz. These curves showed similar behavior to the observed in Fig. 5B. The range of Q (from 35 to 80) observed in Fig. 5B points out that there is a sizeable attenuation in the seismic bandwidth.

To establish the effect of porosity on P wave velocity, new simulations were run in saturated models with different porosity ranging from 2.5% up to 22.5% with a 2.5% variation each. The travel times estimated in depth displayed in Fig. 6A indicate that velocity decreases with porosity (from 3442 m/s in the 1% porosity model to 2093 m/s in the 25% porosity model). The observed variation in velocity coincides with reported velocity-porosity relationships obtained by numerical simulations to derive the elastic properties of model monomineralic consolidated sandstone [17] and empirical dataset of sandstone samples of varying porosity and clay content (from clean to 51% clay) whose velocities were measured at different pressures [18].

The observed velocity-porosity behavior in Fig. 6A was compared to the theoretical velocity models proposed by Wyllie & Gardner [19], Gassmann (1951) [20] and Biot [6], with all their curves plotted in Fig. 6B. The resulting curve shows a linear diminishing trend observed in laboratory research [2]. On one hand, the Wyllie & Gardner curve, which represents a time average equation and not a rigorous theoretical model, defines the upper limit of velocity-porosity relationship. On the other hand, Gassmann´s velocity establishes the lower limit of velocity and coincides with Biot´s velocity in case of a model without tortuosity, that is, entirely connected pores. In the presence of tortuosity, the velocity curve deviates from Gassmann's curve when porosity increases due to the fact that tortuosity affects solid-fluid coupling. The velocity of the rock matrix corresponds to the value where porosity becomes zero, settling around 3700 m/s. This result indicates that when the wave passes through a fully saturated medium, there is a delay in the journey that depends on porosity. Such behavior has also been observed in experimental data and field data [21].

Finally, the isolated effect of saturation in the spectra of amplitude and phase was studied. Fig. 7A shows the amplitude spectra of wavelets recorded in a 10% saturated model with a porosity of 10%. On the surface $\boldsymbol{A_m}$ occurs when $\boldsymbol{f_m}$ is 60 Hz, but as the wave propagates, $\boldsymbol{A_m}$ diminishes while its $\boldsymbol{f_m}$ moves towards lower frequencies. This behavior is accentuated

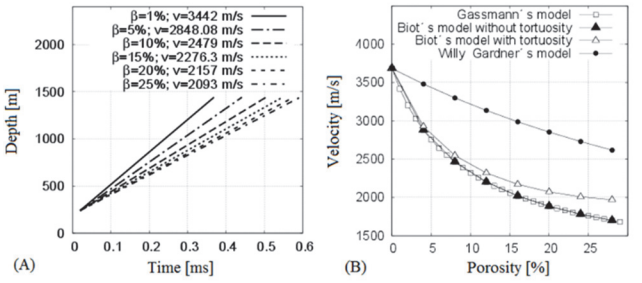

Figure 6 A) Travel times measured across different porosity fully saturated models used to estimate depth-velocity profile. B) Four different velocity-porosity curves provided by different theoretical velocity models together with velocities established in 7A.
Source. The authors.

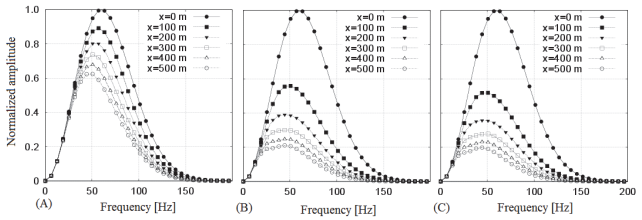

Figure 7. Amplitude spectra in three models with A) 10% saturation, B) 50% saturation, and C) 90% saturation for a model with 15% porosity. The images show that saturation strengthens both the phenomena of attenuation and dispersion.
Source. The authors.

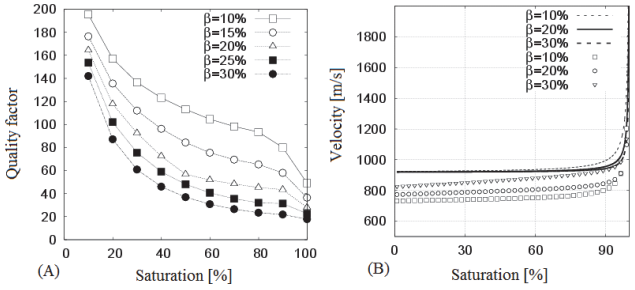

Figure 8 A) Combined effect of porosity and saturation on quality factor, B) Combined effects of porosity and saturation on velocity.
Source. The authors.

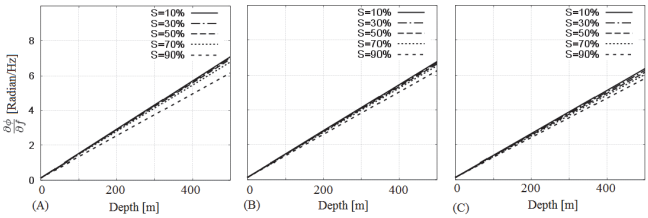

Figure 9. A) 5% porosity models with different saturations, B) 15% porosity models with different saturations, and C) 25% porosity models with different saturations. The images show $\partial\emptyset/\partial f$ diminishing slightly with saturation.
Source. The authors.

when saturation reaches 50% in same model seen in Fig. 7B, where a bi-modal shape appears in a more attenuated spectrum. Fig. 7C shows a stronger effect due to a higher saturation. It can thus be concluded that saturation strengthens both the phenomena of attenuation and dispersion.

Simulations were run on models with porosities of 10%, 15%, 20%, 25% and 30%, with saturations of 10%, 20%, 30% and so on until reaching 99.9%. In each spectra in depth, the quality factors at 60 Hz were estimated and the results, summarized in Fig. 8A, show that the quality factor decreases with saturation and porosity. However, it can be noted that the saturation effect on the quality factor is more intense for saturations below 40%. Above this value, a trend is depicted that is less steep. Furthermore, Fig. 8A shows that the effect of porosity on the quality factor is steeper for lower values with a limiting Q curve of around 22%. In Fig. 8B, the combined effect of porosity and saturation on velocity is observed. When saturation is less than 90%, the propagation velocity remains almost insensitive to saturation, but exceeding that value, velocity increases rapidly until reaching full saturation. A similar behaviour of velocity with water saturation in experimental tests has been reported [22] (Winkler and Murphy, 1995). The extremely low bulk modulus of gas makes it feasible to compress the rock-fluid aggregate, keeping an almost constant velocity. Thus, velocity is mainly affected by porosity and to a lesser extent by saturation except when saturation is almost full. Finally, the influence of saturation on $\boldsymbol{m(z) = \partial\emptyset/\partial f}$ was studied by analyzing the phases observed in the previous simulations. The results are shown in Figs. 9A, 9B and 9C and outline a linear relationship between the increase of $\boldsymbol{\partial\emptyset/\partial f}$ and travel time. Slopes in the set of Figs. 9A, 9B and 9C show that $\boldsymbol{\partial\emptyset/\partial f}$ decreases slightly with saturation. Conversely, Fig. 3B shows that $\boldsymbol{\partial\emptyset/\partial f}$ increases with porosity. Porosity increases the change of phase with frequency and simultaneously saturation slows this effect down but only

4. Conclusions

The propagation of P-wave in porous media that model porous sandstone containing gas and water was numerically simulated allowing for the characterization of the effects of porosity and saturation on velocity, attenuation, and dispersion. When a wave propagates in saturated media, the maximum amplitude of the spectrum shifts to lower frequencies. As a result, sizeable Biot´s losses in seismic bandwidth were observed with low Q values that contradict the belief regarding its absence. Attenuation increases as porosity, saturation and frequency increase but it tends asymptotically towards a limit value. Moreover, when porosity and saturation increase, Q diminishes. Although usually discarded, the phase analysis did provide interesting results. On one hand, the phase varies with frequency with a rate that increases when wavelets propagate. On the other hand, this rate is almost insensitive to saturation but increases with porosity. This term $\boldsymbol{\partial\emptyset/\partial f}$ might be considered a seismic attribute and therefore a porosity indicator.

Finally, a relationship between acoustic wave velocity and fully saturated porosity was established. When saturation is less than 90%, the propagation velocity remains almost constant, but when that value is exceeded, velocity increases rapidly until reaching full saturation.

Acknowledgements

The authors would like to thank Universidad Nacional de Colombia for the support given to this research, especially to the Graduate Program in Geophysics. This paper is a partial result obtained by the physicist Alejandro Duitama, while preparing his Master's thesis in Geophysics.

Bibliography

[1] Sams, M., Neep, J., Worthington, M. and King, M., The measurements of velocity dispersion and frequency-dependent intrinsic attenuation in sedimentary rocks. Geophysics, 62, pp. 1456-1464, 1997. DOI: 10.1190/1.1444249.

[2] White, J., Computed seismic speeds and attenuation in rocks with partial gas saturation. Geophysics, 40, pp. 224-232, 1975. DOI: 10.1190/1.1440520.

[3] Carcione, J., Helle, H. and Pham, N., White's model for wave propagation in partially saturated rocks. Comparison with poroelastic numerical experiments. Geophysics, 68, 1389-1398., 2003. DOI: 10.1190/1.1598132.

[4] Tisato, N., Quintal, B., Chapman, S., Madonna, C., Subramaniyan, S., Frehner, M., Saenger, E. and Grasselli, G., Seismic attenuation in partially saturated rocks. Recent advances and future directions. The Leading Edge, 33(6), pp. 648-655, 2014.

[5] Biot, M., Theory of propagation of elastic waves in a fluid-saturated porous solid, I. Low frecuency range. J. Acous. Soc. Am., 28, pp. 168-178, 1956. DOI: 10.1121/1.1908239.

[6] Biot, M., Theory of propagation of elastic waves in a fluid-saturated porous solid. II. Higher-frecuency range. J. Acous. Soc. Am., 28, pp. 179-191, 1956. DOI: 10.1121/1.1908239

[7] Dvorkin, J., Mavko, G. and Nur, A., Squirt flow in fully saturated rocks. Geophysics, 60, pp. 97-107, 1995. DOI: 10.1190/1.1443767.

[8] Mavko, G. and Nur, A., Wave attenuation in partially saturated rocks. Geophysics, 44, pp. 161-178, 1979. DOI: 10.1190/1.1440958.

[9] Williams, K., Jackson, D., Thorsos, E., Tang, D. and Shock, S., Comparison of sound speed and attenuation measured in sandy sediments to predictions based on the Biot theory of porous media. IEEE, J. Ocean. Eng., 27, pp. 413-428, 2002.

[10] Johnson, D., Theory of frequency dependent acoustics in patchy-saturated porous media. J. Acous, Soc. Am., 110, pp. 682-694, 2001. DOI: 10.1121/1.1381021.

[11] Pride, S. and Berryman, J., Linear dynamics of double porosity and dual-permeability materials. I. Governing equations and acoustic attenuation. Phys. Rev. E., 68, pp. 036603, 2003. DOI: 10.1103/PhysRevE.68.036603.

[12] Pride, S. and Berryman, J., Linear dynamics of double porosity and dual-permeability materials. II. Fluid transport equations. Phys. Rev. E., 60, pp. 4285-4299, 2003.

[13] Caspari, E., Qi, Q., Lopes, S., Gurevich, B., Rubino, J., Velis, D., Clenell, M. and Muller, T., Wave attenuation in partially saturated porous rocks – New observations and interpretation across scales. The Leading Edge, 33(6) pp. 606-614, 2014.

[14] Camarasa, M., Contribución a la teoría de Biot sobre propagación de ondas acústicas en sedimentos saturados en una mezcla de fluidos. Tesis Doctoral, Universidad Complutense de Madrid, Madrid, España,1992.

[15] Duitama, A., Simulación de la atenuación de frecuencias en ondas sísmicas primarias, MSc. Tesis, Departmento de Geociencias, Universidad Nacional de Colombia, Bogotá, Colombia, 2013.

[16] Zeng, Y., He, J. and Liu, W., The application of the perfectly matched layer in numerical modeling of wave propagation in poroelastic media. Geophysics, 6(4), pp. 1258-1266, 2001. Doi: 10.1190/1.1487073.

[17] Knackstedt, M., Arns, C. and Pinczewskiz, W., Velocity-porosity relationships, 1. Accurate velocity model for clean consolidated sandstones. Geophysics, 68, pp. 1822-1834, 2003.

[18] Han, D., Nur, A. and Morgan, D., Effects of porosity and clay content on wave velocities in sandstones. Geophysics, 51, pp. 2093-2107, 1986. DOI: 10.1190/1.1442062.

[19] Wyllie, M. and Gardner, L.W., Elastic wave velocities in heterogeneous and porous media, Geophysics, 21, pp 41-70, 1956. DOI: 10.1190/1.1438217.

[20] Gassmann, F., Uber die elastiziat poroser medien, Vier. der Natur. Gesellschaft, 96, pp 1-26, 1951.

[21] Korneev, V., Goloshubin, M., Daley, T. and Silin, G., Seismic low-frequency effects in monitoring fluid-saturated reservoirs. Geophysics, 69, pp. 522-532, 2004. DOI: 10.1190/1.1707072.

[22] Winkler, K. and Murphy, W., Acoustic velocity and attenuation in porous rocks, in T. Ahrens, ed. Rock physics and phase relations, Reference Shelf 3, AGU, pp 20-34,1955.

A. Duitama-Leal, is Physicist, and MSc. of Geophysics from Universidad Nacional de Colombia. Experience like instructor of physics and mathematics. Knowledge in geophysics and interest in research, particularly in numeric methods and simulation of physics and geophysics systems using the C++ language and parallel programming. In Geophysics, the topics are modeling of wave field, fluids mechanic and seismic theory inversion. ORCID. 0000-0002-5477-2191

O. Almanza-Montero, received the Dr, in Physic in the Universidad de Valladolid (Spain - 2000), his MSc. In Physic in the Universidad Nacional de Colombia. Currently he is professor in this University, from 1996. His works are focused in materials science such as semiconductor and antioxidant activity of some Colombian fruits as well. He is author of more than 50 paper published in different journals. Characterization techniques (XRD, EPR, IR, UV-vis) are methods he usually use. ORCID. 0000-0002-5141-6079

L. Montes-Vides, is Physicist from the Universidad Nacional de Colombia, MSc. in Engineering from the Universidad Nacional de Colombia in 1987 and Dr. in Science – Geophysics from the Universidade Federal do Pará (Brazil - 1998). At the Universidad Nacional de Colombia – sede Bogotá since 1990 as a lecturer in the following programs. undergratuate program in Geology, graduate programs in Master Science in Geophysics and Doctorate in Geosciences, all of them at the Faculty of Sciences. Research areas focused in Seismic prospecting, seismic inversion, seismic modeling and applied computing mathematics. Reviewer of following scientific journals. ESRJ, Revista da SBGf, J.Appl. Geophysics and CT&F. ORCID. 0000-0002-7470-9202